Metallophysics and Advanced Technologies
Металофіз. новітні технол.
Metallofiz. Noveishie Tekhnol.
2021, vol. 43, No. 12, pp. 1653–1665
https://doi.org/10.15407/mfint.43.12.1653
Reprints available directly from the publisher

PACS numbers: 61.72.Dd, 61.72.Ff, 61.72.Hh, 62.20.mj, 62.20.mt, 62.20.Qp

Structure Monitoring of the LaB_6–TiB_2 Composites

O. P. Karasevska[*,**], T. O. Soloviova[**], and P. I. Loboda[**]

[*]*G. V. Kurdyumov Institute for Metal Physics, N.A.S. of Ukraine,*
36 Academician Vernadsky Blvd.,
UA-03142 Kyiv, Ukraine
[**]*National Technical University of Ukraine*
'Igor Sikorsky Kyiv Polytechnic Institute',
37 Peremohy Ave.,
UA-03056 Kyiv, Ukraine

The structure and properties of bulk and powder LaB_6–TiB_2 composites as a promising material in solar energy converters have been studied by X-ray, metallographic, and pulsed excitation methods. The phase composition and defects of the composite's structure have been determined. The effect of heating–cooling cycles (20–1400°C) on the structure's characteristics of the composite's matrix phase is shown. The compatibility of the structure's analysis results by destructive (X-ray and metallographic) and non-destructive methods (pulsed excitation have been established). The capabilities of the pulsed excitation method for determining the composites structural characteristics and using it to control their quality under operating conditions are demonstrated.

Key words: bulk, powder, composite, solar energy, structure, defects, cracks.

Будова та властивості об'ємних та порошкоподібних композитів LaB_6–TiB_2, як перспективного матеріалу в сонячних перетворювачах енергії, вивчені методами рентґенівського аналізу, металографії та імпульсного збудження. Визначено фазовий склад та дефекти структури композиту. Показано вплив циклів нагрівання та охолодження (20–1400°C) на характеристики структури фази матриці композитів. Встановлено сумісність результатів аналізу структури деструктивними (рентґенівським та мета-

Corresponding author: Tetyana Oleksandrivna Soloviova
E-mail: tsolov_1@ukr.net

Citation: O. P. Karasevska, T. O. Soloviova, and P. I. Loboda, Structure Monitoring of the LaB_6–TiB_2 Composites, *Metallofiz. Noveishie Tekhnol.*, **43**, No. 12: 1653–1665 (2021), DOI: 10.15407/mfint.43.12.1653.

лографічним) та неруйнівним (імпульсного збудження) методами. Продемонстровано можливості методу імпульсного збудження для визначення структурних характеристик композитів та використання його для контролю їхньої якості у робочих умовах.

Ключові слова: об'ємний і порошковий композити, сонячна енергія, структура, дефекти, тріщини.

(Received June 1, 2021; in final version, October 8, 2021)

1. INTRODUCTION

New technical designs, which include solar energy converters (SEC), especially require fundamental development of new materials and assessment of their reliability. The results in this area of creating SEC materials and structures require their adaptation to severe load and harsh environmental conditions: automobile and sidewalk solar roads are already being designed and built [1].

Lanthanum hexaboride (LaB_6) is a well-known thermionic material and its ability to emit electrons has been widely used for a long time to create hot cathodes for a wide range of applications, mainly in single crystal form [2, 3]. The previous investigations indicate that LaB_6 is a promising material for solar radiative filters, innovative high-temperature solar absorbers in thermodynamic solar plants, photoelectron ionisation detectors, concentrating solar thermionic systems *et al*. [4–6].

The solar energy converter must also have good mechanical strength and stability under cyclic temperature changes. High fragility and insufficient plasticity are significant disadvantages of LaB_6, which is eliminated by creating LaB_6–(Ti, Zr, Hf, Ta)B_2 composite materials [7–9]. The use of reinforced LaB_6–MeB_2 ceramics makes it possible to increase the efficiency of solar energy converters by increasing the temperature in solar energy concentration systems from the current 800 K to 1100–1200 K. The TiB_2 solar absorbance α is higher than that of other borides (*e.g.* ZrB_2 and TaB_2), while the spectral selectivity α/ε is higher than that of SiC and lower than ZrB_2 and TaB_2 [7]. In the temperature range of 1100–1200 K, the thermal expansion coefficient is the closest in LaB_6 and TiB_2 phase components of the composite in comparison with other diborides [10], which ensures the compatibility of deformation of the phase components of the LaB_6–TiB_2 composite and is a significant advantage for its application.

In addition, TiB_2 has a lower density than ZrB_2, which makes constructions easier and more affordable [7]. For solar cell elements can use the LaB_6–TiB_2 composite both as a compacted powder and as a bulk material. Therefore, another serious problem in understanding the structural behaviour of material and structure SEC under load is a

scaled comparison of their structural behaviour from the micro- and mesolevels to the macrolevel.

Regardless of the method used to obtain a bulk compact LaB_6–TiB_2 composite (hot pressing of powders, laser sintering, self-propagating synthesis, crystallization, or another method) at a density level exceeding 95% of the theoretical value, the main issue is the preservation of its properties with temperature becomes control of structural characteristics and defects. Understanding these effects is important for the development of methods for complete control of the properties of both the material and the design as a whole.

The structural characteristics of composites can be investigated by different methods, which can be divided into two large groups: destructive and non-destructive methods. Metallographic and X-ray methods make it possible to determine the phase composition of materials, the orientation and dislocation structure of crystals are well known and belong to destructive research methods [11–13].

Non-destructive methods based on fibre optic sensors [14], using impulse excitation technique (IET) [15–18], are successfully applied to control structure parameters during deformation and to identify damage. Non-destructive testing methods allow detecting defects associated with structural and phase distortions in laboratory samples and real designs. In this work, we studied bulk and powdered LaB_6–TiB_2 eutectic polycrystalline composites on thin sections of samples and without them in order to compare the results obtained by destructive and non-destructive methods regarding the phase state, structural and mechanical characteristics of the composites.

2. METHODS

Bulk LaB_6–TiB_2 eutectic composites (FZM) are obtained by crucible-free float zone melting on a 'Crystal 206' induction device at a speed of 3 mm/min in a helium medium of 0.1 MPa using a LaB_6 polycrystalline seed [9]). Spherical LaB_6–TiB_2 powders of the eutectic composite ~200 μm in diameter are obtained by centrifugal plasma atomization (AC—atomized composite) of a compressed mixture of LaB_6 and 11 wt.% TiB_2 powders in the eutectic ratio of phase components with the addition of 2 at.% B [19] (Fig. 1).

Microstructure of the composites is studied by scanning electron microscopy REM 106I. X-ray structural analysis (XRD) is performed on an Ultima IV diffractometer (Rigaku, Japan, with Rietveld phase analysis software) using monochromatic CuK_α radiation. Two XRD methods, based on 'θ–2θ' scanning and studying the intensity distribution of spots (I**q**) in the method of reciprocal space mapping (RSM), are used for phase and structural analysis of composites. 'θ–2θ' scanning is carried out by moving the samples with a step of 0.02° in 2θ and

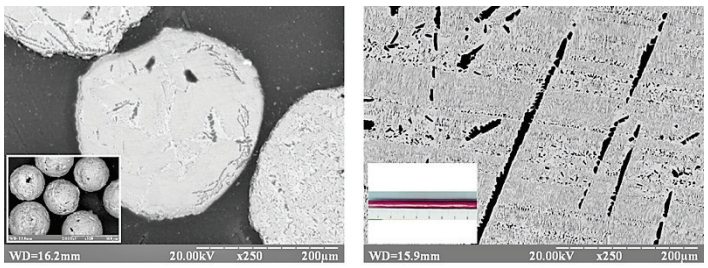

a *b*

Fig. 1. General view and macrostructure of powder (*a*) and bulk (*b*) LaB_6–TiB_2 composites after crystallization.

a measurement time of 4 s/step. In the RSM method, the sample is sequentially moved with a step of 0.01° along two mutually perpendicular axes (ω_1 and ω_2) with an exposure of 2 s/step. The $I\mathbf{q}$ intensity and width (ω_{qn}) of RSM diffraction spots in the azimuthal plane depends on the homogeneity, type, density and location of dislocations in the material and varies depending on the direction, according to [13]:

$$\omega_{q\perp n} \sim \sum_i \rho_i \phi_{in}(b_i, \tau_i, q), \tag{1}$$

where b_i is the Burgers vector of a dislocation from the i-th slip system; ρ_i is the dislocation density; τ_i is the orientation of dislocation lines; ϕ_{in} is the orientation factor, q is the diffraction vector. The accuracy of the angular distribution spots is 5′–9′ with a 0.95 confidence probability.

The dependence of internal friction, or damping (Q^{-1}) and a dynamic elastic modulus (E_d) on temperature has been studied by impulse excitation technique (IET), which has been described in detail elsewhere [15, 16]. The high temperature IET tests are carried out inside an HTVP–1750°C graphite furnace in an Ar atmosphere with a heating and cooling rate of 5°C/min between room temperature and 1400°C, using carbon wires to suspend the samples. The results are analyzed using the RFDA program (IMCE, Genk, Belgium). Through the crystals, sound voltages are transmitted at a frequency of 105 Hz, which allows fixing changes in the material associated with the spectrum of relaxation processes.

Microhardness is measured by Vickers pyramidal indentation (Model FV-700, Future-Tech Corp., Tokyo, Japan) with time exposure of 15 s, and averaging 10 measurements under a load of 30 N. The indentation fracture resistance, K_{1C}, is calculated by the empirical formula [20]:

$$K_{1C} \sim 0.16 HV \alpha^{1/2} (c/\alpha)^{-3/2}, \tag{2}$$

with α, half the diagonal of the indentation (*m*); *HV*, the microhardness of the material (GPa) and *c*, the length of the radial crack (m). Accuracy microhardness measurement (Δ*HV*, %) largely depends on the length of the crack spread values and varies depending on the uniformity of the stress state of the material.

3. RESULTS AND DISCUSSION

3.1. Phase State of Powdered and Bulk LaB_6–TiB_2 Composites After Crystallization

Figure 2 shows the X-ray diffraction patterns and microstructures of the AC and FZM LaB_6–TiB_2 composites. The phase composition of AC powders is represented by two phases: $LaB_6 \pm x_1$ and $TiB_2 \pm x_2$ (where $x_1 \leq 0.14$, and $x_2 \leq 0.09$) (Fig. 2, *a*, line *1*), and individual inclusions of LaB_4 phases are very rarely found in the microstructure (Fig. 2, *b*). In FZM bulk composites the phase composition is also represented by two phases $LaB_6 \pm x_3$ and $TiB_2 \pm x_4$, which, however, somewhat stronger than in AC powders, deviate from the equilibrium eutectic composition ($(x_3 \leq 0.18)$, $(x_4 \leq 0.11)$ and contain ~3–7% additional LaB_4 (~2–4 wt.%) and La_mB_n, Ti_yB_z, (~1–3 wt.%) phases (Fig. 2, *a*, line *2*) [19].

Additional phases are located mainly at the grain boundaries of the matrix phase and, more rarely, inside its grains. The appearance of unstable phases in FZM composites can be caused by a discrepancy between the direction of the predominant crystal growth and the direction of the temperature gradient at the crystallization front. Under AC crystallization, the seed does not limit the direction of crystallization, and it coincides with the direction of the maximum temperature gradient. In this case, the characteristic size of the diffusion zone is commensurate with the radius of curvature of the liquid-solid interface, which reduces concentration overcooling.

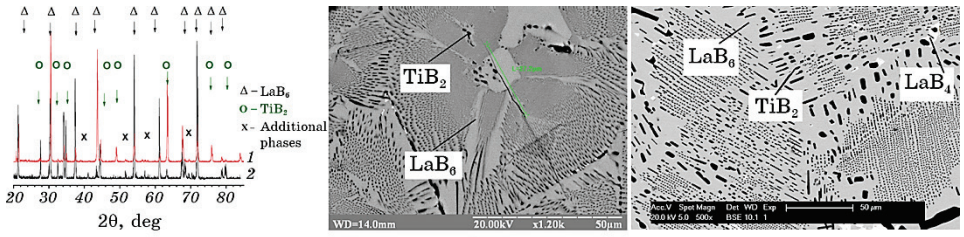

Fig. 2. Diffraction patterns (θ–2θ) (*a*) and microstructures (*b*, *c*) of powdered (*a*, line *1* and *b*) and bulk (*a*, line *2* and *c*) LaB_6–TiB_2 composites in as-grown state.

3.2. Structure of Bulk and Powder LaB_6–TiB_2 Composites After Crystallization

When FZM and AC composites are cooled from the crystallization temperature, the effects of inhomogeneous plastic deformation of its coherently connected components appear. This deformation is determined by differences in the properties of the phase components of composites: coefficients of thermal expansion, elastic moduli, density, strength, stresses due to the discrepancy between the direction of predominant growth with the direction of the maximum temperature gradient, *etc*. As a result, residual stresses (RS) and dislocation substructure of the phase components are formed. RSM studies have shown,

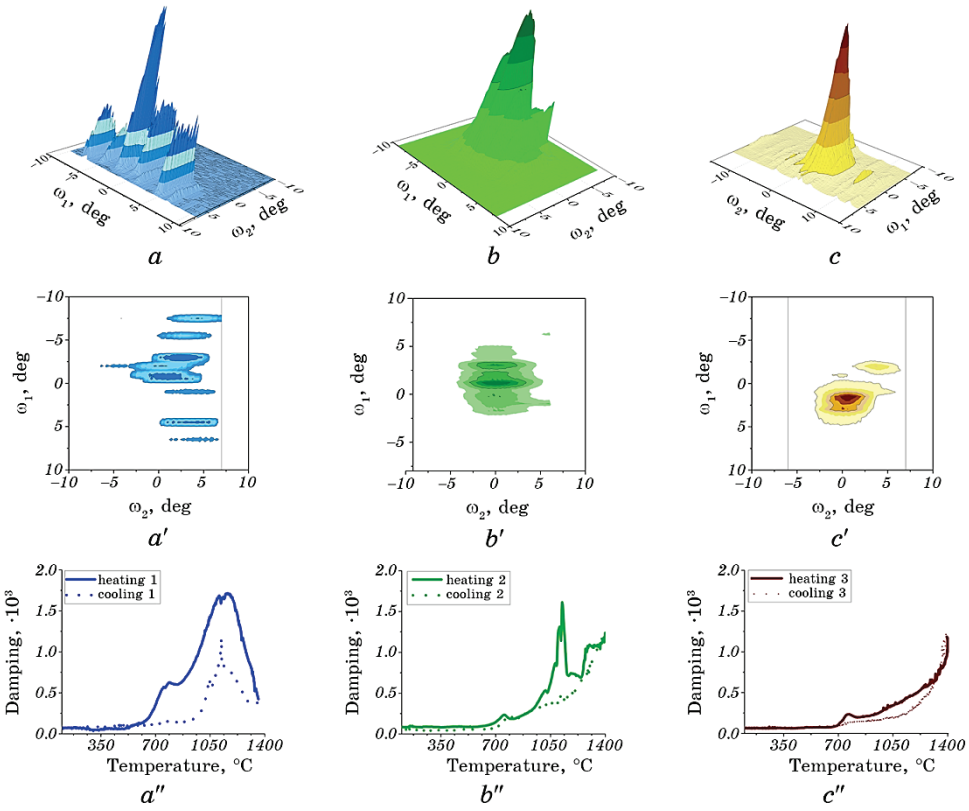

Fig. 3. Typical 3D (*a*, *b*, *c*) and 2D (*a*′, *b*′, *c*′) $I\mathbf{q}_\perp$ distributions of the (100) LaB_6 spots and damping (*a*″, *b*″, *c*″, solid—heating, dots—cooling) of the LaB_6–TiB_2 composite. *a*, *a*′—as-grown state; *b*, *b*′—after the first cycle heating–cooling; *c*, *c*′—after the second cycle heating–cooling; *a*″—the first cycle heating–cooling, *b*″—the second cycle heating–cooling; *c*″—the third cycle heating–cooling.

that in the grains of the matrix phase of the FZM composites in the initial state, the $I\mathbf{q}_\perp$ distributions of diffraction spots are divided by boundaries into separate areas—fragments (Fig. 3, *a*). The intensity of the $I\mathbf{q}_\perp$ distribution between the fragments drops almost to the background values and disorients the substructure of the composites by ~8°–14° in the ω_1 direction (Fig. 3, *a*, *a*′). In the opposite direction (ω_2), the disorientation of the substructure is much less (~1.5°–2°) and is associated with the rotation of fragments by 'geometrically necessary' dislocations that form subgrains.

Based on the shape and width of the $I\mathbf{q}_\perp$ distributions for the matrix phase of the FZM LaB_6–TiB_2 composite, such a distribution can be characterized as a multilevel misoriented structure [21]. In accordance with [13], at the upper mega-level, the matrix phase of the composite is bent by dislocation–disclination boundaries with misorientation angles of ~1.5°–2° between its individual fragments. In turn, the fragments are misoriented by 'geometrically necessary' dislocations that form subboundaries with a misorientation of ~0.2°–0.5° onto subgrains. The dislocation density in subgrains is ~10^9 cm^{-2}. In AC composites, after crystallization, a misoriented substructure also appears, and the $I\mathbf{q}_\perp$ intensity distribution for the matrix phase is shown in Fig. 4, *c*, *d*. The total width $I\mathbf{q}_\perp$ of distributions in AC composites is substantially asymmetric ($\omega'_2 >> \omega'_1$) and is similar to the $I\mathbf{q}_\perp$ distributions in fragments of FZM composites. Figures 4, *a*, *b* show 3D and 2D plots of the $I\mathbf{q}_\perp$ fragment of the matrix phase from Fig. 3, *a*, *a*′.

Because of crystallization in the LaB_6–TiB_2 FZM composites, a

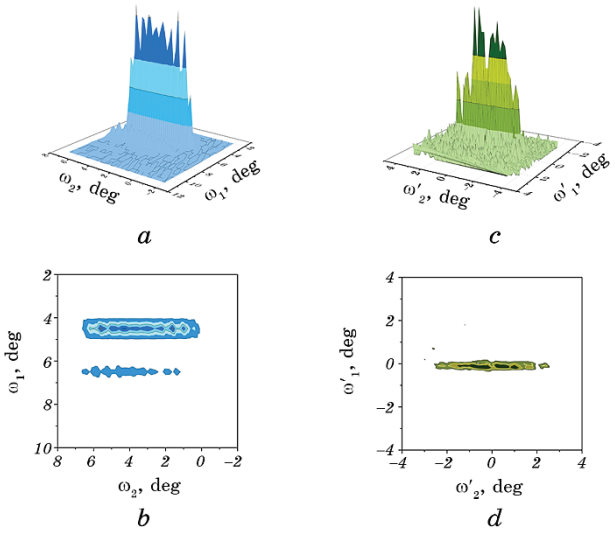

Fig. 4. Typical 3D (*a*, *c*,) and 2D (*b*, *d*) $I\mathbf{q}_\perp$ distributions of the (100) LaB_6 spots of a fragment of FZM (*a*, *b*) and AC (*c*, *d*) composites.

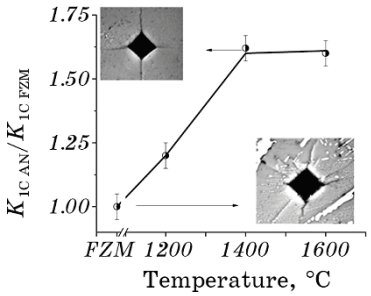

Fig. 5. Change in relative fracture toughness after and before annealing of the LaB_6–TiB_2 composite measured using an indentation force of 30 N.

mixed disclination–dislocation ensemble with localized RS zones is formed. In AC composites, there is also a macro-inhomogeneous stress state, which is manifested by the formation of a misoriented substructure. In the zones of localization of tensile stresses, cracks easily propagate and the material is destroyed.

In the matrix phase of the FZM composite in the as-grown state, cracking after indentation of the Vickers pyramid occurs in different directions relative to its diagonals (at angles to the direction of maximum load) [22]. The directions of crack propagation are associated with the presence of localized RS tension zones in the structure of the FZM composites (Fig. 5, FZM as-grown state).

3.3. Temperature Dependence of Damping and $I\mathbf{q}_\perp$ Distribution in Heating–Cooling Cycles of the LaB_6–TiB_2 FZM Composites

Temperature IET tests ($Q^{-1} \sim f(T)$) FZM LaB_6–TiB_2 composites are shown in Fig. 3, *a*″, *b*″, *c*″. In the first heating cycle with an increase in temperature from 20°C to 1400°C on the $Q^{-1} \sim f(T)$ dependence, a wide maximum of damping is observed in the temperature range 650°C–1400°C with noticeable inflections in the region of 700°C–800°C and 1000°C–1300°C (Fig. 3, *a*″, solid line). On cooling, this damping maximum narrows significantly, forming the largest value near $T \sim$ ~ 1100°C (Fig. 3, *a*″, dot line). In the first cycle of heating–cooling of the composites, their structure changes. Typical $I\mathbf{q}_\perp$ distributions after the first heating–cooling cycle are shown in Fig. 3, *b*, *b*′. The misorientation of fragments and subgrains of the matrix phase of the composites significantly decreased, acquiring a shape close to symmetric 2D; $\omega_2 \sim \omega_1$. The intensity $I\mathbf{q}_\perp$ of the distribution between the fragments does not fall to the background level, and the fragments themselves are uniformly misoriented without significant (≤0.2°) reversals due to subboundaries. The wide maximum $Q^{-1} \sim f(T)$ during the first heating corresponds to the interaction of impulse excitation with de-

fects of a multilevel structure with inhomogeneous elastic stress fields. Cooling in the first cycle of the $Q^{-1} \sim f(T)$ dependence occurs in the composite, in which the structure of the matrix phase at the upper mega-level relaxes and no longer experiences inhomogeneous bending distortions.

In the second heating cycle of the LaB_6–TiB_2 composite, the $Q^{-1} \sim f(T)$ dependence basically repeats its form obtained upon cooling in the first cycle, but somewhat narrows and shifts towards a higher temperature with a maximum of $T \sim 1140$°C (Fig. 3, b'', solid line). Several kinks remain on the damping curve, as with the first heating. Cooling in the second cycle is characterized by almost complete absence of damping maximum in the range 1000°C–1200°C (Fig. 3, c'', dot line).

After the second heating–cooling cycle, the typical 2D shape of the $I\mathbf{q}_\perp$ distribution (Fig. 3, c') becomes close to spherical $\omega_2 \cong \omega_1$, and the 3D spatial $I\mathbf{q}_\perp$ distributions (Fig. 3, b') are smooth, without peak. Such changes in the shape and intensity of the $I\mathbf{q}_\perp$ distribution correspond to the resorption and depletion of local stresses in the composite structure. In composites with such a structure, in the third cycle of the IET test, there are insignificant inflections in the $Q^{-1} \sim f(T)$ dependence upon heating, and upon cooling, the dependence of damping with temperature is monotonic without a damping peak (Fig. 3, c'').

Damping at increased RS has signs of microplasticity and the maxima on the oscillation–damping curve correspond to scattering at the structural boundaries in the first and second IET cycles. The third IET test takes place under the conditions of the formed equilibrium substructure of the composite and the damping peaks have practically disappeared. Under conditions of such a structure, crack resistance also increases. Under the load of the pyramid during Vickers identification, cracks only in the directions of maximum loading along the tops of its indentation are formed (Fig. 5, 1400°C).

Damping, as one of the properties of metallic materials, is primarily determined by the density of dislocations, different mobility of screw and edge dislocations, their segments and bends, and the mobility of anchoring points, which is especially pronounced in inhomogeneous dislocation structures of materials. The movement of dislocations in real crystals leads to a whole set of relaxation linear and nonlinear effects. The effect of annealing on these relaxation processes is different: some peaks of internal friction are annealed, while others can remain up to very high temperatures [23]. What these peaks have in common is that they are relaxation peaks of internal friction characteristic of the rearrangement of dislocation structures. The observed dislocation hysteresis on the $Q^{-1} \sim f(T)$ dependence upon cooling can probably be explained within the framework of the vibrating string model [24], by the interaction of dislocations with mobile defects that are present in a multilevel dislocation structure. This interaction de-

pends on the ratio of the tear stress of dislocations from the boundary with different mobility of anchoring points to the magnitude of stresses in the IET method at a given temperature and vibration frequency. Relaxation effects, which are manifested in the form of peaks of the $Q^{-1} \sim f(T)$ dependence in FZM LaB_6–TiB_2 composites, have a dislocation nature, which is confirmed by RSM studies. Temperature hysteresis restructuring of the microstructural features of the composite upon application of a dynamic load in IET tests causes a change in internal friction, and, consequently, in its elastic properties. Each inflection and peak on the $Q^{-1} \sim f(T)$ curve characterizes the local mobility of individual structural elements of the composite. Thus, the main mechanism of the dissipation of impulse excitation energy in IET tests is the rearrangement of the multilevel system of the composite, transferring its non-equilibrium state to equilibrium.

3.4. Temperature Dependence of the Dynamic Modulus of Elasticity (E_d) in the LaB_6–TiB_2 FZM Composite

The E_d values measured by the IET method, in contrast to the static modulus, reflect only the elastic properties of the material without the creep effect, since the stresses arising in the material during sample vibrations in the IET test are very small in magnitude. Consequently, the dependence of E_d on temperature in the IET test expresses its changes without a force effecting on the material. Figure 6 shows the change in E_d in three consecutive IET tests. The dependence of the dynamic modulus of elasticity of the LaB_6–TiB_2 composite with the as-

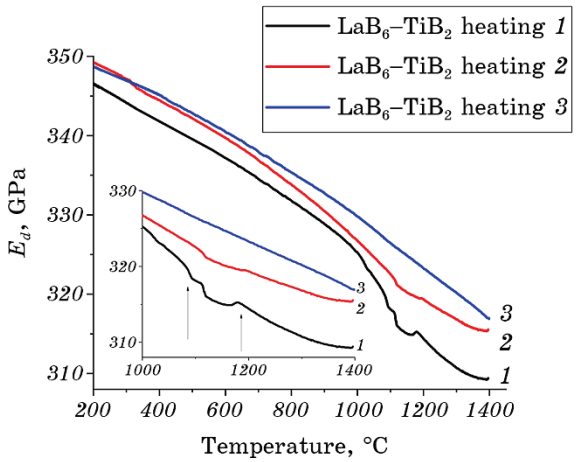

Fig. 6. Temperature dependence of E_d in LaB_6–TiB_2 FZM composite during IET tests. *1*, 2, 3—first, second, and third heating in IET tests.

grown structure as a whole demonstrates a linear change in the temperature range from 20°C to 1400°C ($E_d \sim f(T)$) with features in the range $T \sim$ 1050°C–1250°C and near $T \sim$ 1400°C (Fig. 6, line *1*). The change in $E_d \sim f(T)$ in the range $T \sim$ 1050°C–1250°C has several inflections.

This may be due to the redistribution of the elements of the multilevel dislocation ensemble, supported by the migration of point defects. At $T \geq$ 1000°C in the composite, there is a softening of interatomic bonds in the matrix, and then in the reinforcing fibres, which leads to the appearance of paired equilibrium Schottky–Frenkel defects [25]. Their movement in the region of local stresses in the multilevel dislocation structure of the composite leads to the establishment of an equilibrium, including phase, state of the composite. The relaxation mechanisms of various defects and their complexes are decisive in the change in the physical characteristics of the composite.

In the second IET test, when the LaB_6–TiB_2 composite is heated (Fig. 6, line *2*), $E_d \sim f(T)$ dependence repeats its form during the first heating. Hysteresis of the $E_d \sim f(T)$ dependence is observed, but at much less pronounced fluctuations in the E_d values in the range $T \sim$ ~ 1050°C–1250°C. In our opinion, this is due to a significant decrease in local RS in the multilevel dislocation system, which affects the motion defects and their complexes. As in the case of the first heating, near $T \sim \sim$ 1400°C the dependence $E_d \sim f(T)$ slows down and the value of E_d remains practically constant also. In the third IET test of the composite, $E_d \sim f(T)$ dependence remains linear when heated over the entire temperature range of 20°C–1400°C (Fig. 6, line *3*). This heating of the composite occurs under conditions when the substructure of the matrix phase in the LaB_6–TiB_2 composite has an equilibrium character with practically no local RS, and the phase state corresponds to the eutectic composition.

Studies of the composites structure and properties on samples thin sections and, in general, on a bulk LaB_6–TiB_2 composite show the comparability of the results of the metallographic and X-ray diffraction analyzes with the conclusions of the IET tests regarding the composites structure in the as-grown state, under temperature effects, and the tendency to fracture. The impulse excitation method can be a fast and accurate way to determine the structural characteristics of composites in structures and can be used to control their quality in design, to determine damage and tendency to crack formation.

4. CONCLUSIONS

1. The crystallization structure of FZM and AC LaB_6–TiB_2 composites is a mixed disclination–dislocation ensemble with localized RS zones and reduced crack resistance.
2. Structural analysis of the LaB_6–TiB_2 composites by X-ray, metallo-

graphic, and impulse excitation test provide consistent results for assessing their structural state.

3. Impulse excitation test can be fast and accurate in determining the structural characteristics of composites and used to control their quality in service, determine defects, damage and tendency to crack both the material and the design as a whole.

4. Improvement in the crack resistance of as-grown LaB_6–TiB_2 composites can be obtained with an increase in temperature (≥1400°C) due to softening of interatomic bonds, the creation of equilibrium structural and phase states and enhances the mobility of point defects and dislocations.

REFERENCES

1. K. A. Khan, S.A. Khan, L. Talwar, and Y. S. Chib, *International Journal of Current Research*, **10**, Iss. 5: 69440 (2018).
2. C. Oshima, M. Aono, T. Tanaka, S. Kawai, and R. Shimizu, *J. Appl. Phys.*, **51**: 1201 (1980).
3. M. Futamoto, M. Nakazawa, and U. Kawabe, *Surface Sci.*, **100**, No. 3: 470 (1980).
4. C. Zimmer, J. Schubert, S. Hamann, U. Kunze, and T. Doll, *Phys. status solidi (a)*, **208**, No. 6: 1241 (2011).
5. L. Xiao, Y. Su, W. Qiu, Y. Liu, J. Ran, J. Wu, F. Lu, F. Shao, D. Tang, and P. Peng, *Ceramics International*, **42**, No. 12: 14278 (2016).
6. E. Sani, L. Mercatelli, M. Meucci, L. Zoli, and D. Sciti, *Sci. Rep.*, **7**: 718 (2017).
7. E. Sani, M. Meucci, L. Mercatelli, A. Balbo, C. Musa, R. Licheri, R. Orrù, and G. Cao, *Solar Energy Materials and Solar Cells*, **169**: 313 (2017).
8. K. Hirano, *J. Eur. Ceram. Soc.*, **25**, No. 8: 1191 (2005).
9. P. Loboda, *Powder Metall. Met. Ceram.*, **39**: 480 (2000).
10. T. Soloviova, O. Karasevska, J. Vleugels, and P. Loboda, *Ceramics International*, **47**, No. 12: 17667 (2021).
11. M. Wilkens, *Kristall und Technik*, **11**: 1159 (1976).
12. P. F. Fewster, *Newsletter*, No. 24: 17 (2000).
13. M. A. Krivoglaz, *X-Ray and Neutron Diffraction in Nonideal Crystals* (Berlin-Heidelberg: Springer: 1996).
14. Y. Shan, H. Xu, Zh. Zhou, Z. Y., X. Xu, and Zh. Wu, *J. Intelligent Material Systems and Structures*, **30**, No. 13: 1951 (2019).
15. R. Gibson, *Composites Sci. Technol.*, **60**, No. 15: 2769 (2000).
16. G. Roebben, B. Basu, J. Vleugels, and O. Van der Biest, *J. European Ceramic Society*, **23**, No. 3: 481 (2003).
17. A. Swarnakar, S. Giménez, S. Salehi, J. Vleugels, and O. Van der Biest, *Recent Key Engineering Materials*, **333**: 235 (2007).
18. A. Al-Adnani, F Mustapha, S. Sapuan, and M. Saifulnaz, *J. Intelligent Material Systems and Structures*, **27**, No. 17: 1 (2016).
19. T. Soloviova, O. Karasevska, and P. Loboda, *Ceramics International*, **45**, No. 7: 8677 (2019).

20. A. G. Evans and E. A. Charles, *J. American Ceramic Society*, **59**: 371 (1976).
21. V. Panin, *Mater. Sci. Engineering: A*, **319–321**: 197 (2001).
22. T. Soloviova, O. Karasevska, J. Vleugels, and P. Loboda, *J. Alloys Compd.*, **729**: 749 (2017).
23. A. Seeger, *Mat. Sci. Eng. A*, **370**, No. 1/2: 50 (2004).
24. A Granato and K. Lucke, *J. Appl. Phys.*, **27**, No. 6: 583 (1956).
25. C. Kittel, *Introduction to Solid State Physics* (Wiley: 2004).